

β -Alkyl substituted Dithieno[2,3-*d*;2',3'-*d'*]benzo[1,2-*b*;4,5-*b'*]dithiophene Semiconducting Materials and Their Application to Solution-Processed Organic Transistors

Jonggi Kim,^{†,||} A-Reum Han,^{‡,||} Jung Hwa Seo,[§] Joon Hak Oh,^{*,‡} and Changduk Yang^{*,†}

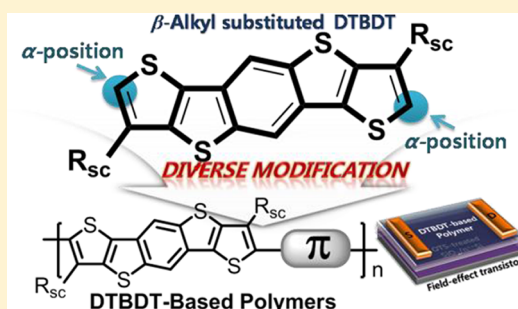
[†]Interdisciplinary School of Green Energy and [‡]School of Nano-Bioscience and Chemical Engineering, KIER-UNIST Advanced Center for Energy (K-U ACE), Low Dimensional Carbon Materials Center, Ulsan National Institute of Science & Technology (UNIST), Ulsan 689-798, South Korea

[§]Department of Materials Physics, Dong-A University, Busan 604-714, South Korea

S Supporting Information

ABSTRACT: A novel highly π -extended heteroacene with four symmetrically fused thiophene-ring units and solubilizing substituents at the terminal β -positions on the central ring, dithieno[2,3-*d*;2',3'-*d'*]benzo[1,2-*b*;4,5-*b'*]dithiophene (DTBDT) was synthesized via intramolecular electrophilic coupling reaction. The α -positions availability in the DTBDT motif enables the preparation of solution-processable DTBDT-based polymers such as PDTBDT, PDTBDT-BT, PDTBDT-DTBT, and PDTBDT-DTDP. Even with its highly extended acene-like π -framework, all polymers show fairly good environmental stability of their highest occupied molecular orbitals (HOMOs) from -5.21 to -5.59 eV. In the course of our study to assess a profile of semiconductor properties, field-effect transistor performance of the four DTBDT-containing copolymers via solution-process is characterized, and PDTBDT-DTDP exhibits the best electrical performance with a hole mobility of $1.70 \times 10^{-2} \text{ cm}^2 \text{ V}^{-1} \text{ s}^{-1}$. PDTBDT-DTDP has a relatively smaller charge injection barrier for a hole from the gold electrodes and maintains good coplanarity of the polymer backbone, indicating the enhanced π - π stacking characteristic and charge carrier transport. The experimental results demonstrate that our molecular design strategy for air-stable, high-performance organic semiconductors is highly promising.

KEYWORDS: dithieno[2,3-*d*, 2',3'-*d'*]benzo[1,2-*b*, 4,5-*b'*]dithiophene, heteroacenes, thiophene-benzene annulated acenes, organic field-effect transistors (OFETs), polymeric semiconductors



INTRODUCTION

Organic field-effect transistors (OFETs) based on π -conjugated organic semiconductors have been intensively investigated as key elements for realizing low-cost, flexible, large-area electronic displays.^{1–13} Owing to the excellent solution processability, film uniformity, and thermal stability, π -conjugated polymeric materials are a promising choice to commercialize OFETs.^{14–23} Among a number of molecular classes reported so far, linearly fused higher oligoacenes, exemplified by pentacene consisting of five fused benzenes, exhibit mobility of up to $3.0 \text{ cm}^2 \text{ V}^{-1} \text{ s}^{-1}$ because of their strong intermolecular π - π interaction in the crystalline state.^{24–26} Spurred by these promising results, Bao et al. reported solution-soluble pentacene-containing conjugated polymers with slightly improved air-stability compared to pentacene itself.²⁷ However, those polymers exhibited very low mobilities of $\sim 8 \times 10^{-7} \text{ cm}^2 \text{ V}^{-1} \text{ s}^{-1}$ in a nitrogen environment and no field-effect behavior in ambient conditions because of their intrinsically insufficient air-stability (the highest occupied molecular orbitals (HOMO) = -5.08 eV).²⁸ As an alternative to the benzene-based acenes, structurally related π -extended cores based on thiophene ring with much better stability have been focused either on

thieno[*n*]acenes^{29–32} or thiophene-benzene annulated acenes^{32,33} for the development of molecular organic semiconductors (see Figure 1). Moreover, in S-containing fused heteroacenes, the nonbonding sulfur–sulfur interaction of neighboring molecules can play an important role in facilitating charge transport in OFETs.^{30–34} Together with consideration of the ability to ink formulations with tuned rheological properties, thereafter, these units as π -cores have also been integrated into conjugated polymers for good OFET characteristics with environmental stability (Figure 1).²⁹ Nonetheless, none of the chemistries are readily applicable to the synthesis of large heteroacene molecules. Recently, Müllen et al. have successfully developed dithieno[2,3-*d*;2',3'-*d'*]benzo[1,2-*b*;4,5-*b'*]dithiophene (DTBDT) derivatives as a five-ring-fused pentacene analogue by using a simple intramolecular electrophilic coupling reaction (see Figure 1).^{35–37} The desirable chemical, electronic, and morphological structures of DTBDT yielded a high hole mobility of up to $1.7 \text{ cm}^2 \text{ V}^{-1} \text{ s}^{-1}$ in

Received: June 12, 2012

Revised: August 15, 2012

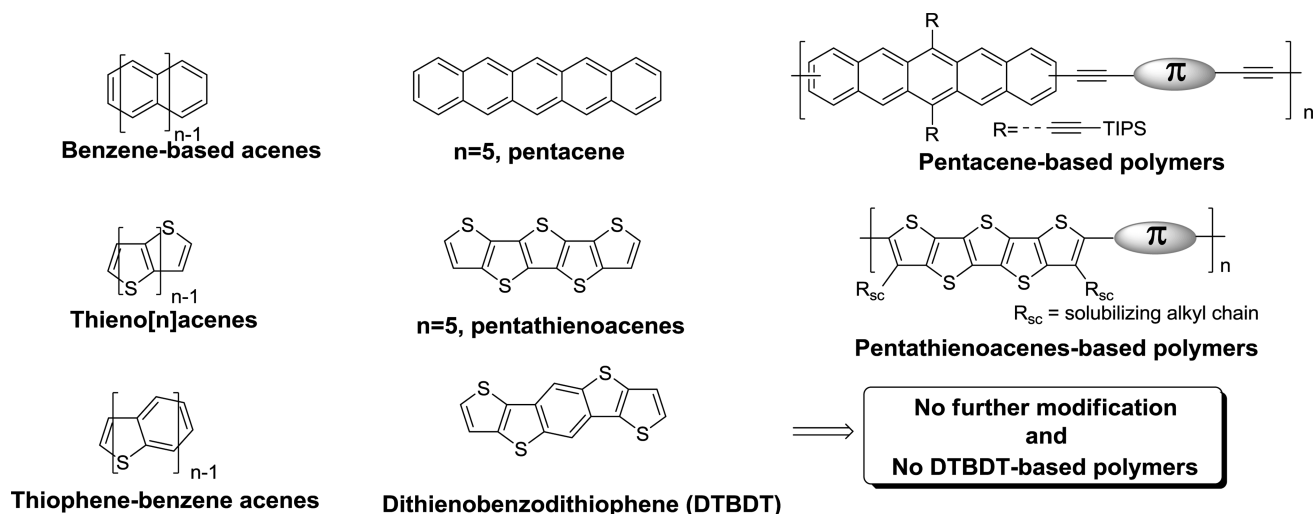


Figure 1. Chemical structures of linear acenes, thieno[n]acenes, thiophene-benzene acenes, and their semiconducting polymers.

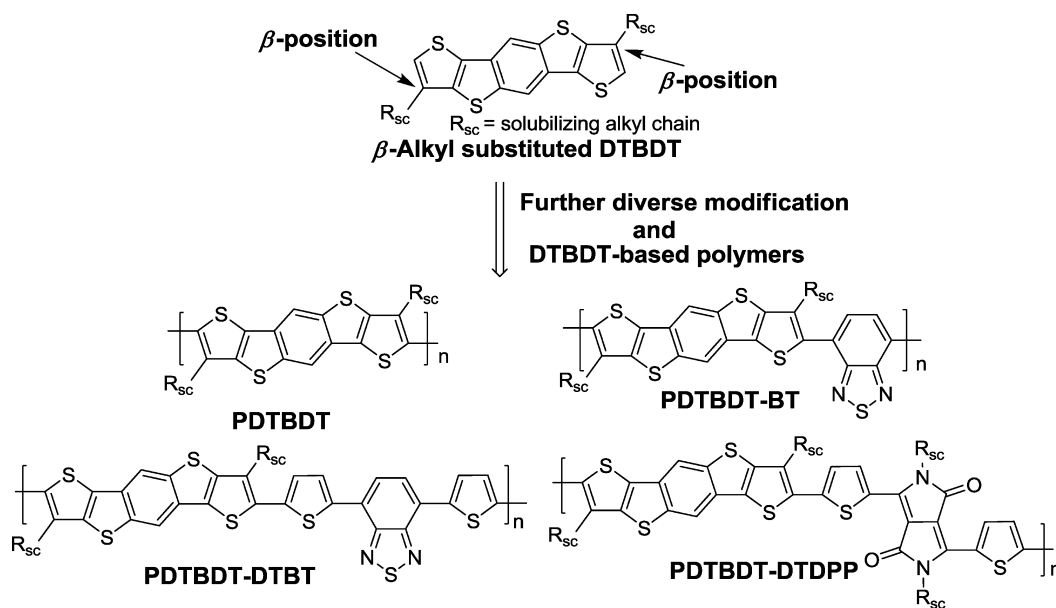


Figure 2. β -alkyl substituted DTBDT and DTBDT-containing polymers.

solution-processed OFETs.³⁷ Besides, the comparison of the relatively low HOMO levels and larger band gaps of DTBDT derivatives to other fused heteroacenes suggested DTBDT motif as one of the most stable oligoacene semiconductors.

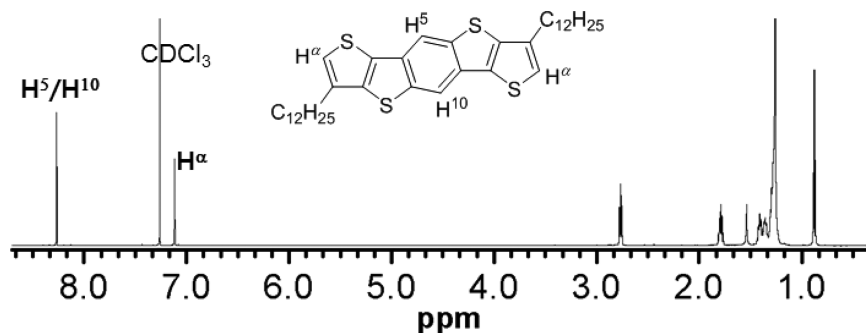
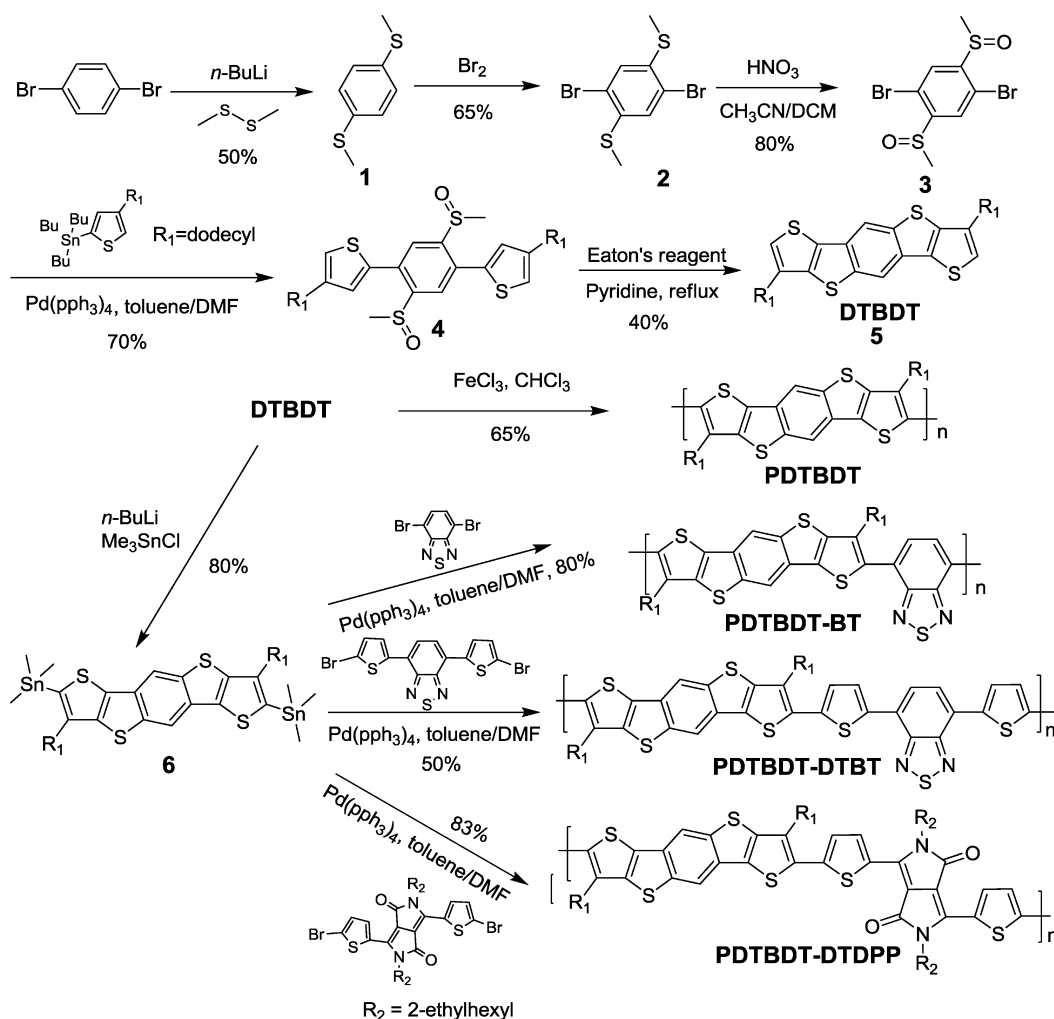
Although further development of the materials based on DTBDTs would be expected to afford superior printable organic semiconductors, their related materials formed by introducing DTBDT moieties into molecules have not been reported so far. This is a result of incorporating the solubilizing substituents at the terminal α -positions of the DTBDT unit, which makes further chemical modification no longer possible.

Replacement of the α -substituents in DTBDT with β -solubilizing groups is a promising strategy to increase the diversity of the modification of the molecular and electronic structures, which can lead to the development of superior organic semiconductors. In this work, we design and effectively synthesize a β -alkyl substituted DTBDT by employing Müllen's previously explained synthetic methodology. The α -positions availability of the resulting DTBDT allows us to prepare various DTBDT-containing polymers. Here, we not only report on a

new polymer semiconductor based on DTBDT but also several commonly used conjugated building blocks such as 2,1,3-benzothiadiazole (BT), 4,7-dithienyl-2,1,3-benzothiadiazole (DTBT), and 3,6-dithiophen-2-yl-pyrrolo[3,4-*c*]pyrrole-1,4-dione (DTDPP) copolymerized with DTBDT units to investigate the relationships between their structures and properties. A series of conjugated polymers, that is, PDTBDT, PDTBDT-BT, PDTBDT-DTBT, and PDTBDT-DTDPP are shown in Figure 2. It should be pointed out that, to the best of our knowledge, β -substituted DTBDT as a building block and its derivatives are so far the first examples synthesized and used for the fabrication of OFET devices.

RESULTS AND DISCUSSION

Synthesis and Characterization. The synthetic routes to the β -alkyl substituted DTBDT monomer and DTBDT-based polymers (PDTBDT, PDTBDT-BT, PDTBDT-DTBT, and PDTBDT-DTDPP) are depicted in Scheme 1. Compounds 1, 2, and 3 were easily prepared in moderate to good isolated yields according to the established methods.³⁸ The key

Scheme 1. Synthetic Routes of β -Dodecyl Substituted DTBDT and DTBDT-Containing Polymers (PDTBDT, PDTBDT-BT, PDTBDT-DTBT, and PDTBDT-DTDP)Figure 3. ^1H NMR spectrum of β -dodecyl substituted DTBDT (CDCl_3 , 600 MHz, 300 K).

intermediate 1,4-dibromo-2,5-bis(methylsulfinyl)benzene **3** effectively cross-coupled with 5-tributylstannyl-3-dodecylthiophene to afford the precursor **4** in a yield of 70%. Dodecyl was chosen as the long side chain of the precursor to ensure good solubility of the target semiconducting molecules in organic solvents and solution processability. In our initial synthetic attempt, the trifluoromethanesulfonic acid induced intramolecular ring-closing reaction of the dimethylsulfinyl benzene with the adjacent thiophene rings was attempted and followed by a reflux in pyridine, but no desired product was observed. A likely rationale for this result is the occurrence of the

intermolecular cross-linking reaction. Thus, the intramolecular ring closure was performed with Eaton's reagent (7.7 wt % P_2O_5 in $\text{CH}_3\text{SO}_3\text{H}$) as a relatively mild Lewis acid at a low concentration, successfully resulting in the regioisomer-free β -dodecyl-substituted DTBDT (**5**) as an off-white solid in 40% yield. As shown in Figure 3, the ^1H NMR spectrum provides unambiguous evidence for no isomers since all the typical singlets can be assigned to the corresponding aromatic protons in the molecule (see the ^{13}C NMR in the Supporting Information for further information). Finally, the organotin DTBDT monomer **6** was synthesized by deprotonation with *n*-

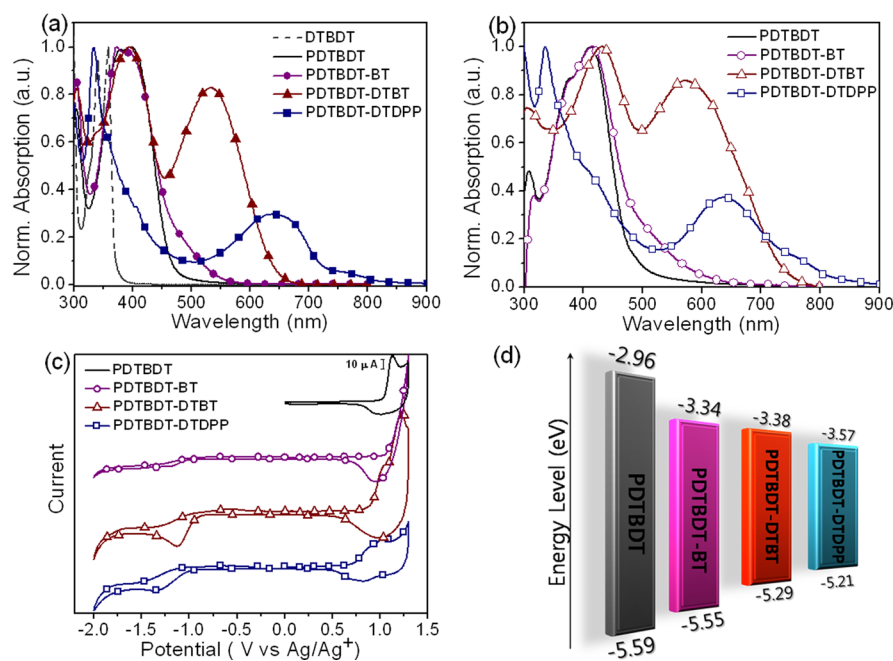


Figure 4. UV-vis absorption spectra of DTBBDT-based polymers in *o*-DCB solution (a) and as thin solid films (b). Cyclic voltammograms of DTBBDT-based polymer thin films (c). Energy level diagrams for DTBBDT-based polymers (d).

Table 1. Optical and Electrochemical Properties of DTBBDT-Based Polymers

polymer	$\lambda_{\text{max}}^{\text{abs}}$ (<i>o</i> -DCB, nm)	$\lambda_{\text{onset}}^{\text{abs}}$ (film, nm)	$E_{\text{g}}^{\text{opt}}$ (film, eV) ^a	HOMO (eV) ^b	LUMO (eV) ^c	$E_{\text{g}}^{\text{elec}}$ (eV) ^d
PDTBBDT	396	411	2.63	-5.59	-2.96 ^e	
PDTBBDT-BT	393	412	2.28	-5.55	-3.34	2.21
PDTBBDT-DTBT	394, 532	431, 572	1.91	-5.29	-3.38	1.90
PDTBBDT-DTDPP	334, 636	335, 636	1.51	-5.21	-3.57	1.64

^aCalculated from onset wavelength in absorption spectra. ^bHOMO = $-(E_{\text{onset}}^{\text{ox}} - E_{1/2}^{\text{ferrocene}} + 4.8)$ eV. ^cLUMO = $-(E_{\text{onset}}^{\text{red}} - E_{1/2}^{\text{ferrocene}} + 4.8)$ eV. ^d $E_{\text{g}}^{\text{elec}}$ (eV) = $E_{\text{onset}}^{\text{ox}} - E_{\text{onset}}^{\text{red}}$. ^eLUMO = $E_{\text{g}}^{\text{opt}} + \text{HOMO}$.

BuLi followed by quenching with trimethyltin chloride, which is capable of functionalization either asymmetrically or symmetrically with various π -cores at both terminal positions of DTBBDT as well as incorporation into versatile oligomers and polymers through metal-mediated cross-coupling reactions. For solution-processable polymeric semiconductors, the DTBBDT-based polymer PDTBBDT was first synthesized by oxidative coupling of DTBBDT using FeCl_3 in anhydrous chloroform. A combination of an electron-rich and an electron-deficient unit in a copolymer main chain is a well-known synthetic strategy to yield low band gap with relatively high charge carrier mobilities due to the intramolecular charge transfer (ICT). Thus, such desirable properties afford the necessary motivation for further work toward the preparation of novel donor-acceptor copolymers based on DTBBDT. Therefore, a series of donor-acceptor polymers, PDTBBDT-BT, PDTBBDT-DTBT, and PDTBBDT-DTDPP were prepared by copolymerizing a newly conceived soluble DTBBDT donor moiety with various acceptor moieties, namely, 2,1,3-benzothiadiazole (BT), 4,7-dithienyl-2,1,3-benzothiadiazole (DTBT), and 3,6-dithiophen-2-ylpyrrolo[3,4-*c*]pyrrole-1,4-dione (DTDPP), respectively. All the polymers were purified by sequential Soxhlet extraction processes with methanol, acetone, and hexane to remove the fractions of small molecules. After purification, the molecular weights of the resulting solids from either chloroform or chlorobenzene fraction were investigated by gel permeation chromatography (GPC) against PS standard (for details, see

Experimental Section). The difference of the molecular weights may result from either the reactivity of the acceptor segments or the different solubility of the resulting polymers. Attempts are underway to attach longer branched alkyl groups to β -positions of DTBBDT than dodecyl groups, which would presumably make the polymers more soluble during polymerization and thus allow the synthesis of high molecular weight polymers. Also, the DTBBDT-based polymers have good thermal stability which was examined by thermogravimetric analysis (TGA) techniques, and these polymers showed a decomposition temperature of about 400 $^{\circ}\text{C}$ under nitrogen atmosphere (Supporting Information, Figure S4a).

Optical and Electrochemical Properties. The UV-vis spectra for four polymers PDTBBDT, PDTBBDT-BT, PDTBBDT-DTBT, and PDTBBDT-DTDPP in *o*-dichlorobenzene (*o*-DCB) solution and as spin-coated films on glass are shown in Figure 4a–b and the absorption maxima (λ_{max}) are summarized in Table 1. Compared with DTBBDT as a small molecule, all polymer solutions show large red-shifts which demonstrates that all the polymers have extended their conjugation through polymer chain formation. In solution, the parent polymer PDTBBDT shows a strong absorption π - π^* transition band at $\lambda_{\text{max}} = 396$ nm, which is mostly identical to that of the as-spun thin film. This suggests that PDTBBDT has a highly ordered backbone structure and strong π - π interaction in the solution because of the flat skeleton.³⁹ On the other hand, the absorption spectra of the DTBBDT-cored donor-

acceptor copolymers (PDTBDT-DTBT and PDTBDT-DTDPP) in the solutions are characterized with two bands, one near 334–394 nm and the other centered at 532–636 nm. The former bands can be assigned to π - π^* transitions whereas the lowest energy bands are due to ICT between the donor and the acceptor moieties. Relative to the solution absorption, the absorption spectrum of PDTBDT-DTBT film is slightly broadened and exhibits a red shift (~ 40 nm), indicating the presence of stronger interactions between molecules (packing effect) in the solid state. However, the absorption of PDTBDT-DTDPP remains almost unchanged from the solution to the film as the similar feature observed from PDTBDT. This implies that there are aggregations of the polymer chains formed in solution that can be accounted for by π - π stacking of fused ring moieties (DTBDT and DPP). Most surprising is that the optical features of PDTBDT-BT in both solution and films reveal remarkable similarity to those of PDTBDT even though PDTBDT-BT has an alternating donor-acceptor bichromophore system. This means that DTBDT is a weak donor unit like other fused aromatic compounds such as naphtho[2,1-*b*:3,4-*b'*]dithiophene (NDT), dithieno[3,2-*f*:2',3'-*h*]quinoxaline (QDT), and benzo[1,2-*b*:4,5-*b'*]dithiophene (BnDT).

The electronic states and ionization potential/electron affinity (HOMO/LUMO levels) of the DTBDT-based polymer films on a Pt electrode were investigated by cyclic voltammetry (CV) (Figure 4c) and the electrochemical data are also listed in Table 1. All polymers exhibit quasi-reversible or reversible *p*-doping/dedoping (oxidation/reduction) processes in the positive potential range, while irreversible *n*-doping/dedoping (reduction/reoxidation) behaviors in the negative potential range are observed. Note that like the other *p*-type fused heteroacene frameworks,³³ as the reduction potentials of PDTBDT are out of our scan range, the lowest unoccupied molecular orbital (LUMO) energy level is calculated from the HOMO energy level and the optical band gap. The reversibility of CV in the oxidation processes can be interpreted as a good sign of the stability of the radical cation of DTBDT. Furthermore, in terms of electrochemical properties, the HOMO level of PDTBDT is empirically estimated to be -5.59 eV, which is lower than those of pentacene and most oligothiophenes. The low-lying HOMO and relatively large band gap afford environmental stability.

Compared with PDTBDT, the HOMO level of PDTBDT-BT (-5.55 eV) is almost unchanged but its LUMO level (-3.34 eV) shows a significant decrease of 0.38 eV, most likely being rationalized by considering the electron-deficient BT species in the polymers. In both cases of PDTBDT-DTBT and PDTBDT-DTDPP, the noticeably higher HOMO levels are ascribed to the two unsubstituted thiophene units in the π -system because these thiophene rings render the resulting conjugated polymer backbone more electron-rich. From these results, we conclude that the insertion of unsubstituted thiophene segments allows a moderate modulation of the band gap and energy level of the resulting polymers. This finding will assist the future design of semiconductive polymers with tunable electronic properties.

DFT Frontier Molecular Energy Calculation. To provide an insight into the molecular architecture of the polymers, a molecular simulation was carried out for the DTBDT-based polymers with a chain length of $n = 1$ using density functional theory (DFT) at the B3LYP/6-31G* with the Gaussian 03 package. To simplify the calculations, the β -dodecyl chains in

the molecular backbone of DTBDT and two 2-ethylhexyl substituents on the DPP are replaced by hydrogen and methyl groups, respectively. As expected from the fused-acene structure of the DTBDT unit, its geometry is entirely planar. In addition, good coplanarity also exists in the DTBDT-containing polymers (PDTBDT, PDTBDT-DTBT, and PDTBDT-DTDPP) (Figure 5). Thus, we propose that they

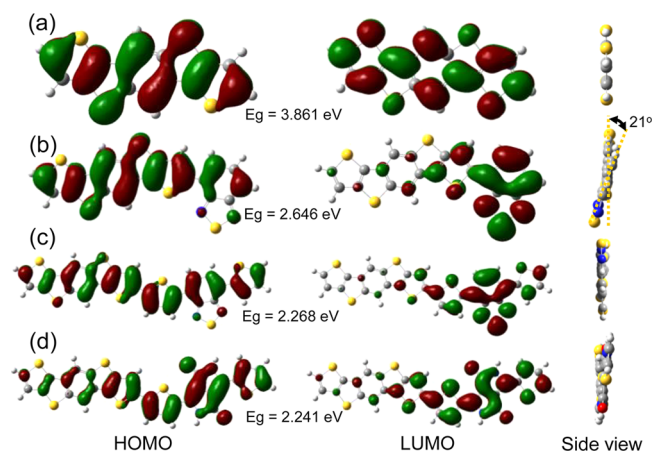


Figure 5. DFT-optimized geometries and charge-density isosurfaces for the HOMO and LUMO levels and the side views of (a) PDTBDT, (b) PDTBDT-BT, (c) PDTBDT-DTBT, and (d) PDTBDT-DTDPP.

will allow efficient π - π stacking between facing backbones and enhance the charge carrier transport in the π - π direction. However, in the case of PDTBDT-BT, steric interactions between directly neighboring BT and DTBDT moieties induce a 21° twist in the ground state of the isolated molecule (Figure 5b), supporting our aforementioned interpretation about absorption features reflecting the absence of ICT in PDTBDT-BT. PDTBDT shows a similar density of states distribution for both the HOMO and LUMO wave functions, implying the weak donor nature of DTBDT. On the other hand, the HOMOs of the donor-acceptor copolymers (PDTBDT-BT, PDTBDT-DTBT, PDTBDT-DTDPP) are well-distributed along the conjugated chains; their LUMOs are centralized on each acceptor unit such as BT, DTBT, and DTDPP, being proposed effective *p*-type organic semiconductors. Theoretical calculations also show that the HOMO-LUMO gaps decrease with the electron-withdrawing abilities of the acceptors groups on the molecules, supporting the notion that DPP possesses enhanced electron-accepting ability relative to BT. Those speculations are in agreement with the optical and electrochemical results above (Table 1). Considering the packing motif and the enhanced ICT effect, we predicted that PDTBDT-DTDPP would give the best performance in OFETs (vide infra).

Morphology and X-ray Diffraction (XRD) Analyses of Thin Films. The morphologies of the DTBDT-based polymer thin films were investigated with atomic force microscopy (AFM). The granular domain sizes in the as-cast polymer thin films became larger upon thermal treatment at 150°C (Figure 6 and Supporting Information, Figure S5). For instance, the as-cast PDTBDT-DTDPP thin film showed randomly entangled and nanofibrillar clusters, whereas the annealed thin film exhibited significantly larger grains, implying enhanced

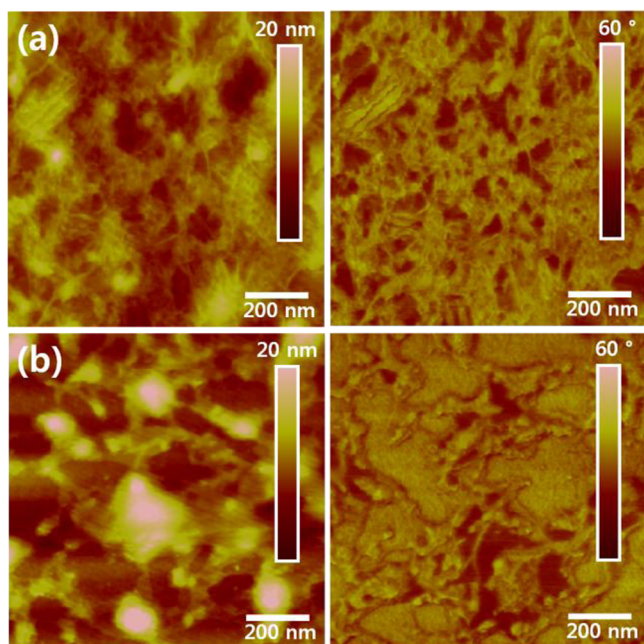


Figure 6. AFM height (left) and phase (right) images of the PDTBDT-DTDPP thin films (a) as-cast, (b) annealed at 150 °C on OTS-treated SiO₂/Si substrates.

intermolecular interactions and potentially facilitated charge transport (Figure 6).

To further elucidate the crystalline nature and molecular orientation in the polymer thin films, out-of-plane X-ray diffraction (XRD) analysis was carried out on the DTBBDT-based polymer thin films. DTBBDT-based polymer thin films display relatively well-defined XRD peaks (Figure 7 and Supporting Information, Figure S6). The out-of-plane $d(001)$ -

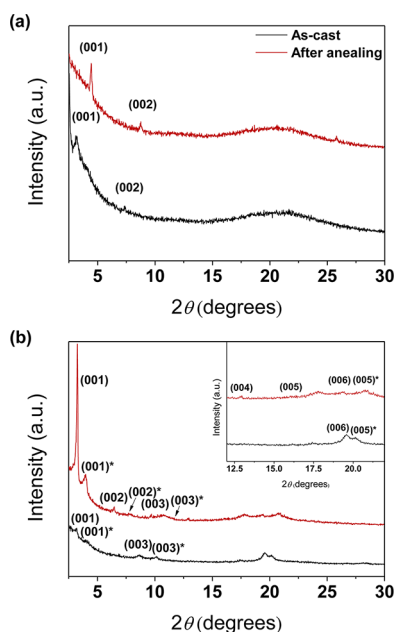


Figure 7. XRD patterns obtained from (a) PDTBDT-BT, (b) PDTBDT-DTDPP thin films as-cast (black) and annealed at 150 °C (red). Symbol * for PDTBDT-DTDPP thin film denotes the secondary phase (P2) of crystalline polymorphs in the polymer thin film.

spacing of polymer thin film was decreased (by up to ~ 7 Å) after thermal treatment, indicating the formation of a denser molecular packing (Supporting Information, Table S1). The annealed PDTBDT thin film exhibited the first, second, and third order diffraction peaks at $2\theta = 4.38^\circ$, 8.72° , 12.92° , respectively, revealing that the film has a relatively long-range order (Supporting Information, Figure S6). PDTBDT-BT and PDTBDT-DTBT thin films showed the primary diffraction peak at $2\theta = 4.44^\circ$ and 4.32° after annealing, corresponding to $d(001)$ -spacing values of 19.89 Å and 20.43 Å, respectively. (Figure 7a and Supporting Information, Table S1). Despite the relatively large dihedral angle (21°) between BT and DTBBDT moieties predicted by our DFT calculations, the crystalline ordering was observed in the thin film. On the other hand, the annealed PDTBDT-DTDPP thin films displayed two primary (001) diffraction peaks at $2\theta = 3.24^\circ$ and 3.94° , corresponding to $d(001)$ -spacing values of 27.24 Å and 22.40 Å, respectively. This reflects the existence of crystalline polymorphs in the polymer thin film. Additional higher order diffraction peaks were observed at larger 2θ , indicating that PDTBDT-DTDPP thin film has the largest long-range order among the DTBBDT-based polymer thin films. The polymorphism of PDTBDT-DTDPP was also investigated using differential scanning calorimetry (DSC) analysis. In the DSC thermogram, two exothermic crystallization peaks were observed, indicating the existence of two polymorphs (See Supporting Information, Figure S4b).

OFET Characterizations. To investigate how the acceptor units copolymerized with DTBBDT affect charge transport, we fabricated bottom-gate/top-contact OFETs. The polymer thin films were drop-cast from a chloroform solution onto *n*-octadecyltrimethoxysilane (OTS)-treated SiO₂/Si substrates. The films were annealed on a hot plate at 150 °C for 30 min in N₂ atmosphere. Further details on the surface treatment and OFET fabrication are included in the Experimental Section. The OFET performance of the annealed thin films of DTBBDT-based polymers is listed in Table 2. All the DTBBDT-based polymers exhibited hole-transporting (*p*-channel) characteristics. The typical transfer characteristics are illustrated in Figure 8 (The typical output characteristics are illustrated in Supporting Information, Figure S8). The annealed thin films of DTBBDT-based polymers showed significantly enhanced mobilities, compared with the as-cast polymer thin films (See Supporting Information, Table S2: typically 10^{-3} – 10^{-8} cm² V⁻¹ s⁻¹ for the as-cast polymer thin films). The average hole mobility of the annealed polymer thin films was found to be in the order of 10^{-2} – 10^{-3} cm² V⁻¹ s⁻¹ except for PDTBDT-BT ($\sim 10^{-4}$ cm² V⁻¹ s⁻¹). This is presumably due to the influence of the torsional hindrance by the BT unit in PDTBDT-BT, which is in line with the results of the DFT calculation. PDTBDT as a homopolymer exhibits a high threshold voltage (V_T) of -55.8 V, probably because of the larger charge injection barrier given by the low-lying HOMO (-5.59 eV).⁴⁰ PDTBDT-DTBT showed a relatively higher mobility than PDTBDT-BT. This can be attributed to the fact that two unsubstituted thiophene units adjacent to the BT unit truly reduce the influence of torsional hindrance and enhance coplanarity of the polymer backbone. Among the DTBBDT-based polymers, PDTBDT-DTDPP exhibited the best OFET performance with a hole mobility as high as 1.70×10^{-2} cm² V⁻¹ s⁻¹ and a reasonably small V_T of -7.1 V. PDTBDT-DTDPP has a relatively smaller charge injection barrier for hole from the gold electrodes because of the well-matching HOMO

Table 2. OFET Performance of DTBBDT-Based Polymer Thin Films Annealed at 150 °C

polymer	μ_{\max} [$\text{cm}^2 \text{V}^{-1} \text{s}^{-1}$]	μ_{avg} [$\text{cm}^2 \text{V}^{-1} \text{s}^{-1}$]	$I_{\text{on}}/I_{\text{off}}$	V_T [V]
PDTBBDT	3.40×10^{-3}	1.94×10^{-3}	6.40×10^4	-55.8
PDTBBDT-BT	4.53×10^{-4}	3.18×10^{-4}	4.27×10^5	-24.7
PDTBBDT-DTBT	1.13×10^{-2}	9.24×10^{-3}	1.42×10^4	-22.5
PDTBBDT-DTDPP	1.70×10^{-2}	1.54×10^{-2}	4.98×10^4	-7.1

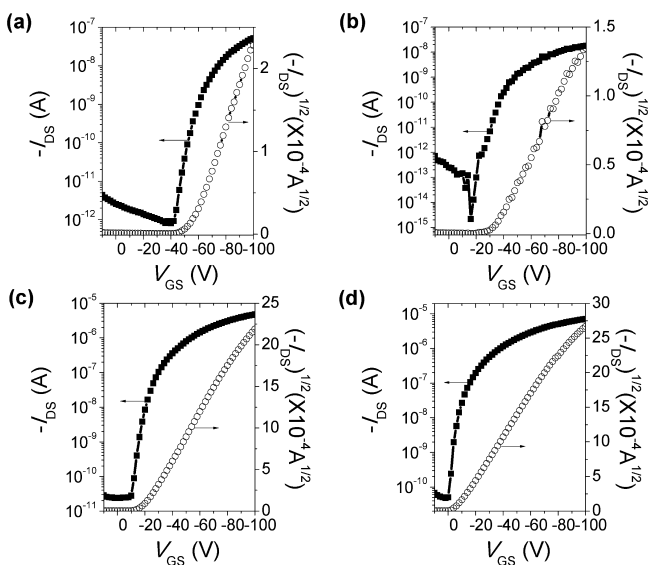


Figure 8. Transfer characteristics of OFET devices of DTBBDT-based polymers annealed at 150 °C ($V_{\text{DS}} = -100$ V); (a) PDTBBDT, (b) PDTBBDT-BT, (c) PDTBBDT-DTBT, and (d) PDTBBDT-DTDPP.

level. In addition, introduction of a DPP segment to the copolymer backbone allows a long-range molecular ordering in the polymer thin films, as shown by X-ray diffraction (XRD) analysis. These electrochemical and molecular packing characteristics of PDTBBDT-DTDPP thin films are found to facilitate charge transport.

CONCLUSIONS

In summary, a soluble weak donor, β -dodecyl substituted DTBBDT, which is a highly π -extended heteroacene with four symmetrically fused thiophene-ring units, has been synthesized via intramolecular electrophilic coupling reaction. The α -positions availability of the DTBBDT enable us to obtain the parent polymer as well as to create “weak donor–acceptor” copolymers by incorporating various electron-deficient comonomers. Despite their highly extended aromatic features, four DTBBDT-based polymers (PDTBBDT, PDTBBDT-BT, PDTBBDT-DTBT, and PDTBBDT-DTDPP) exhibit noticeably low-lying HOMO energy levels (-5.21 to -5.59 eV), implying fairly good environmental stability. The XRD patterns and AFM images for the surface morphology show that thermally treated DTBBDT-based polymer thin films have enhanced intermolecular interactions, thereby facilitating charge transport in the thin-film transistor setting. The solution-processed OFETs using DTBBDT-based polymers as an active layer exhibit p -channel characteristics, and the PDTBBDT-DTDPP exhibits the best electrical performance with a hole mobility of $1.70 \times 10^{-2} \text{ cm}^2 \text{V}^{-1} \text{s}^{-1}$ and a small V_T of -7.1 V because of the small charge injection barrier from the electrodes and excellent coplanarity of the polymer backbone. High hole mobility, air stability, and ease of structural modification make

the DTBBDT an excellent candidate as a new class of p -type semiconductors. Further studies to optimize DTBBDT-based devices are under way.

EXPERIMENTAL SECTION

Materials and Instruments for Characterizations. All reagents and chemicals were purchased from Sigma-Aldrich chemical company and used without further purification. THF was freshly distilled over sodium and benzophenone, prior to use. ^1H and ^{13}C NMR were recorded on Varian VNRS 600 MHz spectrophotometer using the deuterated chloroform (CDCl_3) with TMS as an internal standard. Elemental analyses of carbon, hydrogen and sulfur were carried out with Flash 2000 elemental analyzer, and MALDI-TOF spectra were measured with a Bruker Ultraflex III. To investigate molecular weights and polydispersity indices (PDI) of new polymers, gel permeation chromatography (GPC) was carried out with Agilent 1200 series and miniDAWN TREOS using tetrahydrofuran (THF) as solvent against PS as a standard. UV–vis absorption spectra were recorded on a Varian Carry 5000 spectrophotometer at room temperature. Cyclic voltammetry (CV) measurement was performed on AMETEK VersaSTAT 3 with a three-electrode cell in a nitrogen bubbled 0.1 M tetra-*n*-butylammonium hexafluorophosphate ($n\text{-Bu}_4\text{NPF}_6$) solution in acetonitrile at a scan rate of 50 mV/s at room temperature. As electrodes, the Ag/Ag $^+$ (0.1 M of AgNO $_3$ in acetonitrile) reference electrode, a platinum counter electrode, and polymers coated platinum working electrodes were used respectively. The Ag/Ag $^+$ reference electrode was calibrated using a ferrocene/ferrocenium redox couple as an internal standard, whose oxidation potential is set at -4.8 eV with respect to zero vacuum level. The HOMO energy levels were obtained from the equation $\text{HOMO} = -(E_{\text{ox}}^{\text{onset}} - E_{(\text{ferrocene})}^{\text{onset}} + 4.8)$ eV. The LUMO levels of polymers were obtained from the equation $\text{LUMO} = -(E_{\text{red}}^{\text{onset}} - E_{(\text{ferrocene})}^{\text{onset}} + 4.8)$ eV. The surface topographic images on the films were acquired in the tapping mode using a Veeco Multimode V AFM. All measurements were made at room temperature in ambient conditions. XRD analysis for all of the films was performed with a Bruker D8 Advance high resolution X-ray diffractometer.

OFET Device Preparation and Measurement. Highly n -doped (100) Si wafers ($<0.004 \text{ } \Omega\text{-cm}$) with a thermally grown SiO $_2$ (300 nm, $C_i = 10 \text{ nF cm}^{-2}$) were cleaned with piranha solution and UV-ozone plasma. The surface of SiO $_2$ /Si wafer was modified with octadecyltrimethoxysilane (OTS) as previously reported.^{41,42} 3 mM of OTS solution, prepared by using trichloroethylene (TCE) as the solvent, was placed to cover the entire surface of SiO $_2$ /Si substrate on a spin coater. After waiting for at least 10 s, spin coating was performed at 3000 rpm for 30 s. The wafer was then placed into a larger desiccator in which a vial filled with NH $_4$ OH (1–2 mL) was put together. House vacuum was applied to the desiccator for 5 min, and the whole system was set aside in ambient conditions for 12 h. The samples were removed, and washed sequentially with toluene, acetone, isopropyl alcohol, and then dried using a nitrogen gun. DTBBDT-based polymers were dissolved in chloroform (5 mg mL^{-1}) and stirred at 50 °C for 24 h. The prepared polymer solution was drop-cast onto the hydrophobic OTS-treated SiO $_2$ /Si, and placed in a vacuum oven at 50 °C for 12 h. Then, the polymer film (~ 35 nm) was annealed on a hot plate at 150 °C for 30 min under N $_2$ atmosphere. Au (40 nm) was deposited to form source and drain electrodes with a channel length (L) of 50 μm and a channel width (W) of 1000 μm . The OFET characteristics were measured in a N $_2$ -filled glovebox by using a Keithley 4200 semiconductor parametric analyzer. The field-effect mobility was calculated in the saturation regime using the following equation:

$$I_{DS} = \frac{1}{2}(W/L)\mu C_i(V_G - V_T)^2$$

where I_{DS} is the drain-to-source current, μ is the mobility, and V_G and V_T are the gate voltage and threshold voltage, respectively.

Synthesis of 5,5'-(2,5-Bis(methylsulfanyl)-1,4-phenylene)bis(3-dodecylthiophene) (4). A dry 250 mL three-neck flask was flushed with argon and charged with the compound 3 (5.0 g, 13.88 mmol) and 5-tributylstannyl-3-dodecylthiophene (15.8 g, 29.14 mmol) in anhydrous solvent of toluene (60 mL) and DMF (15 mL). Pd(pph₃)₄ (0.8 g, 0.69 mmol) was added and then the mixture was refluxed overnight. Reaction progress was monitored by TLC. The reaction was quenched with water, which was followed by washing with dichloromethane several times. After drying it over MgSO₄ and concentrated in vacuo, the crude was purified by column chromatography (silica gel, dichloromethane) to afford white solid product (6.9 g, 70%). ¹H NMR (CDCl₃, 600 MHz): δ ppm 8.16 (s, 2H), 7.13 (s, 2H), 7.05 (s, 2H), 2.63 (t, $J = 7.8$ Hz, 4H), 2.54 (s, 6H), 1.63 (t, $J = 7.2$ Hz, 4H), 1.33–1.26 (m, 36H), 0.87 (t, $J = 7.2$ Hz, 6H). ¹³C NMR (CDCl₃, 150 MHz): δ ppm 147.07, 144.52, 136.94, 132.54, 129.68, 125.94, 122.77, 41.68, 31.90, 30.46, 30.39, 29.65, 29.63, 29.60, 29.43, 29.33, 29.24, 22.67, 14.10. MALDI-TOF (m/z) calcd: 703.2; found: 703.23. Elemental analysis calcd for C₄₀H₆₂O₂S₄: C, 68.32; H, 8.89; O, 4.55; S, 18.24 Found: C, 68.02; H, 8.60; S, 17.98.

Synthesis of 3,8-Didodecylidithieno[2,3-d;2',3'-d']benzo[1,2-b;4,5-b']dithiophene (5). The compound 4 (3.0 g, 4.26 mmol) was stirred with Eaton's reagent (25 mL) at room temperature under dark for 3 days. The mixture was poured into ice-water and dark brown solid collected by suction-filtration was dried in vacuum oven. A dry 250 mL three-neck flask was flushed with argon and charged with the brown sulfonium salt, which was followed to be redissolved in pyridine (100 mL) and then the mixture was refluxed overnight. When the reaction mixture turned red, it was cooled down. After extracting with a large volume of dichloromethane, the separated organic phase was dried over MgSO₄ and solvent was removed in vacuo. The crude was purified by column chromatography on silica gel using dichloromethane as an eluent. Finally, recrystallization from hexane gave off-white powder (1.10 g, 40%). ¹H NMR (CDCl₃, 600 MHz): δ ppm 8.26 (s, 2H), 7.11 (s, 2H), 2.76 (t, $J = 7.2$ Hz, 4H), 1.79 (t, $J = 7.2$ Hz, 4H), 1.42–1.25 (m, 36H), 0.87 (t, $J = 7.2$ Hz, 6H). ¹³C NMR (CDCl₃, 150 MHz): δ ppm 139.98, 138.92, 136.10, 133.17, 130.58, 122.28, 115.39, 31.83, 29.76, 29.57, 29.54, 29.46, 29.30, 29.26, 29.24, 28.77, 22.57, 13.92. MALDI-TOF (m/z) calcd: 639.1; found: 639.23. Elemental analysis calcd for C₃₈H₅₄S₄: C, 71.41; H, 8.52; S, 20.07 Found: C, 71.71; H, 8.56; S, 19.87.

Synthesis of 2,7-Bis(trimethylstannyl)-3,6-didodecylidithieno[2,3-b;2',3-b']benzo[1,2-b;4,5-b']dithiophene (6). The compound 5 (0.83 g, 1.29 mmol) flushed with argon in a 250 mL Schlenk flask was dissolved with freshly distilled THF (100 mL). *n*-BuLi (1.6 M, 2.43 mL, 3.87 mmol) was added dropwise to the mixture at -78 °C. After stirring for an hour, trimethyltin chloride (1.03 g, 5.16 mmol) was added in one portion at -78 °C. The reaction mixture was allowed to warm to room temperature and stirred overnight. The reaction was quenched with water, and the organic phase was separated after washing with dichloromethane several times. After drying over MgSO₄, solvent was removed in vacuo. The caramel-like phase (1.0 g, 80%) was obtained as product, and this was used for polymerization without any further purification. ¹H NMR (CDCl₃, 600 MHz): δ ppm 8.21 (s, 2H), 2.76 (t, $J = 7.8$ Hz, 4H), 1.75 (t, $J = 7.8$ Hz, 4H), 1.42–1.26 (m, 36H), 0.88 (t, $J = 7.2$ Hz, 6H), 0.46 (s, 18H). ¹³C NMR (CDCl₃, 150 MHz): δ ppm 142.64, 140.40, 140.00, 138.91, 136.30, 130.02, 115.70, 32.20, 31.93, 30.16, 29.73, 29.68, 29.65, 29.54, 29.49, 29.36, 22.69, 14.12, -7.72 . MALDI-TOF (m/z) calcd: 964.7; found: 964.09. Elemental analysis calcd for C₄₄H₇₀S₄Sn₂: C, 54.78; H, 7.31; S, 13.30; Sn, 24.61. Found: C, 54.90; H, 7.29; S, 13.21.

Synthesis of Poly[3,8-didodecylidithieno[2,3-b;2',3-b']benzo[1,2-b;4,5-b']dithiophen-2,7-diyl] (PDTBDT). FeCl₃ (200 mg, 1.23 mmol) was placed in a 100 mL Schlenk flask. The compound 5 (200 mg, 0.31 mmol) in 30 mL of anhydrous chloroform was added with stirring under argon. The dark mixture was stirred at room temperature for 2 days. The reaction mixture was poured into MeOH/NH₄OH (4:1).

After stirring for 24 h, brown powder was collected by filtration. The powder was purified by Soxhlet extraction with MeOH, acetone and hexane in sequence. Aqueous EDTA solution was treated for the chloroform fraction. The separated phase was concentrated and poured into MeOH. Finally, the light brown polymer (130 mg, 65%) was collected by filtration and vacuum-dried. GPC analysis: $M_n = 17,000$ g/mol, $M_w = 52,000$ g/mol, and $M_w/M_n = 3.05$ (for only THF-soluble fraction, against PS standard). ¹H NMR (CDCl₃, 600 MHz): δ ppm 8.26 (br, 2H), 2.88–2.78 (br, 4H), 2.16–2.0 (br, 4H), 1.45–1.08 (br, 36H), 0.87–0.84 (br, 6H).

Synthesis of Poly[3,8-didodecylidithieno[2,3-b;2',3-b']benzo[1,2-b;4,5-b']dithiophen-2,7-diyl-alt-2,1,3-benzothiadiazole-4,7-diyl] (PDTBDT-BT). The compound 6 (200 mg, 0.20 mmol) and 4,7-dibromo-2,1,3-benzothiadiazole (58.8 mg, 0.20 mmol) in a tube-type Schlenk flask were dissolved with anhydrous mixture of toluene (8 mL)/DMF (2 mL). After bubbling with argon for 10 min, Pd(pph₃)₄ (11.55 mg, 0.01 mmol) was added and then the mixture was refluxed for 2 days. The reaction mixture was poured into MeOH to precipitate into red powder, which was followed by filtration. The collected powder was purified by Soxhlet extraction with MeOH, acetone, and hexane in sequence. The fraction from chloroform was washed with aqueous DETA solution for 10 h. Finally, the concentrate phase was poured into MeOH to afford a red polymer (120 mg, 80%). GPC analysis: $M_n = 16,500$ g/mol, $M_w = 35,500$ g/mol, and $M_w/M_n = 2.15$ (for only THF-soluble fraction, against PS standard). ¹H NMR (CDCl₃, 600 MHz): δ ppm 8.28–12 (br, 2H), 7.94–7.88 (br, 2H), 2.81 (br, 4H), 1.94–1.79 (br, 4H), 1.25 (br, 36H), 0.85 (br, 6H).

Synthesis of Poly[3,8-didodecylidithieno[2,3-b;2',3-b']benzo[1,2-b;4,5-b']dithiophen-2,7-diyl-alt-4,7-dithienyl-2,1,3-benzothiadiazole-2',5'-diyl] (PDTBDT-DTBT). The compound 6 (200 mg, 0.20 mmol) and 4,7-di(2'-bromothien-5'-yl)-2,1,3-benzothiadiazole (96.2 mg, 0.21 mmol) in a tube-type Schlenk flask were dissolved with anhydrous toluene (6 mL) and DMF (1.5 mL) under argon. After addition of Pd(pph₃)₄ (12.13 mg, 0.01 mmol), the reaction mixture was refluxed for 2 days. The mixture was poured into MeOH to precipitate dark red powder. After filtration, the powder was washed in sequence with MeOH for 1 day and acetone for 1 day by Soxhlet extraction. EDTA aqueous solution was treated for chloroform and chlorobenzene fraction. Final precipitation in MeOH gave dark red polymer (20 mg for chloroform fraction and 80 mg for chlorobenzene fraction, 50%). GPC analysis: $M_n = 9,000$ g/mol, $M_w = 16,500$ g/mol, and $M_w/M_n = 1.83$ (for only THF-soluble fraction, against PS standard). ¹H NMR (CDCl₃, 600 MHz): δ ppm 8.27–8.14 (br, 2H), 7.98–7.71 (br, 2H), 7.52–7.32 (br, 4H), 3.04–2.53 (br, 4H), 2.06–1.62 (br, 36H), 0.88–0.83 (br, 6H).

Synthesis of Poly[3,8-didodecylidithieno[2,3-b;2',3-b']benzo[1,2-b;4,5-b']dithiophen-2,7-diyl-alt-2,5-diethylhexyl-3,6-dithiophen-2-yl-pyrrolo[3,4-c]pyrrole-1,4-dione-5',5''-diyl] (PDTBDT-DTDP). The compound 6 (200 mg, 0.20 mmol) and 3,6-bis(5-bromothiophen-2-yl)-2,5-bis(2-ethylhexyl)pyrrolo[3,4-c]pyrrole-1,4-dione (136 mg, 0.20 mmol) were placed in a tube-type Schlenk flask connected with argon. The mixture was dissolved with anhydrous toluene (6.5 mL) and DMF (1.5 mL). Pd(pph₃)₄ (11.55 mg, 0.01 mmol) as a catalyst was added into the mixture and then the reaction mixture was heated up with stirring to reflux for 2 days. The mixture was poured into MeOH/NH₄OH (4:1) to precipitate green powder. Soxhlet extraction was performed in sequence with MeOH and acetone for 1 day each to remove small molecules and collect the chloroform fraction. From final precipitation in MeOH gave green polymer powder (200 mg, 83%). GPC analysis: $M_n = 16,500$ g/mol, $M_w = 59,000$ g/mol, and $M_w/M_n = 3.57$ (for only THF-soluble fraction, against PS standard). ¹H NMR (CDCl₃, 600 MHz): δ ppm 9.09 (br, 2H), 8.30–8.10 (br, 2H), 7.14–7.08 (br, 2H), 3.75–3.73 (br, 4H), 3.01–2.75 (br, 4H), 2.03–1.99 (br, 1H), 1.82–1.77 (br, 4H), 1.40–1.08 (br, 52H), 0.96–0.83 (br, 18H).

■ ASSOCIATED CONTENT

Supporting Information

¹H and ¹³C NMR spectra of monomers. TGA, DSC, AFM, and XRD data. Output characteristics of DTBDT-based polymers

on FET. This material is available free of charge via the Internet at <http://pubs.acs.org>.

AUTHOR INFORMATION

Corresponding Author

*E-mail: yang@unist.ac.kr (C.Y.), joonhoh@unist.ac.kr (J.H.O.).

Author Contributions

[†]The first two authors contributed equally to this work.

Notes

The authors declare no competing financial interest.

ACKNOWLEDGMENTS

This work was supported by the National Research Foundation of Korea (NRF) grant (Code Nos.: 2010-0002494, 2010-0019408, 2010-0026163, 2010-0026916, 2011-0026424, 2011-0017174) funded by the Korean Government (MEST), and by a grant (Code No.: 2011-0031628) from the Center for Advanced Soft Electronics under the Global Frontier Research Program of the MEST, Korea.

REFERENCES

- (1) Klauk, H. In *Organic Electronics: Materials, Manufacturing and Applications*; Wiley-VCH Verlag GmbH & Co. KGaA: Weinheim, Germany, 2006.
- (2) Bao, Z.; Locklin, J. In *Organic Field-Effect Transistors*; CRC Press: Boca Raton, FL, 2007.
- (3) Anthony, J. E.; Facchetti, A.; Heeney, M.; Marder, S. R.; Zhan, X. W. *Adv. Mater.* **2010**, *22*, 3876.
- (4) Crone, B.; Dodabalapur, A.; Lin, Y. Y.; Filas, R. W.; Bao, Z.; LaDuca, A.; Sarpeshkar, R.; Katz, H. E.; Li, W. *Nature* **2000**, *403*, 521.
- (5) Murphy, A. R.; Fréchet, J. M. J. *Chem. Rev.* **2007**, *107*, 1066.
- (6) Bao, Z.; Rogers, J. A.; Katz, H. E. *J. Mater. Chem.* **1999**, *9*, 1895.
- (7) Boudreault, P. L. T.; Wakim, S.; Tang, M. L.; Tao, Y.; Bao, Z.; Leclerc, M. *J. Mater. Chem.* **2009**, *19*, 2921.
- (8) Cho, S.; Lee, J.; Tong, M. H.; Seo, J. H.; Yang, C. *Adv. Funct. Mater.* **2011**, *21*, 1910.
- (9) Lee, J.; Cho, S.; Seo, J. H.; Anant, P.; Jacob, J.; Yang, C. *J. Mater. Chem.* **2012**, *22*, 1504.
- (10) Lee, J.; Cho, S.; Yang, C. *J. Mater. Chem.* **2011**, *21*, 8528.
- (11) Treier, M.; Liscio, A.; Mativetsky, J. M.; Kastler, M.; Müllen, K.; Palermo, V.; Samori, P. *Nanoscale* **2012**, *4*, 1677.
- (12) El Gemayel, M.; Treier, M.; Musumeci, C.; Li, C.; Müllen, K.; Samori, P. *J. Am. Chem. Soc.* **2012**, *134*, 2429.
- (13) Wang, S.; Kiersnowski, A.; Pisula, W.; Müllen, K. *J. Am. Chem. Soc.* **2012**, *134*, 4015.
- (14) Sivaramakrishnan, S.; Chia, P. J.; Yeo, Y. C.; Chua, L. L.; Ho, P. K. H. *Nat. Mater.* **2007**, *6*, 149.
- (15) Garnier, F.; Hajlaoui, R.; Yassar, A.; Srivastava, P. *Science* **1994**, *265*, 1684.
- (16) Leclerc, M.; Morin, J.-F. *Design and Synthesis of Conjugated Polymers*; Wiley-VCH Verlag GmbH & Co. KGaA: Weinheim, Germany, 2010.
- (17) Sirringhaus, H. *Adv. Mater.* **2005**, *17*, 2411.
- (18) Yan, H.; Chen, Z. H.; Zheng, Y.; Newman, C.; Quinn, J. R.; Dotz, F.; Kastler, M.; Facchetti, A. *Nature* **2009**, *457*, 679.
- (19) Tsao, H. N.; Cho, D.; Andreasen, J. W.; Rouhanipour, A.; Breiby, D. W.; Pisula, W.; Müllen, K. *Adv. Mater.* **2009**, *21*, 209.
- (20) Zhang, M.; Tsao, H. N.; Pisula, W.; Yang, C.; Mishra, A. K.; Müllen, K. *J. Am. Chem. Soc.* **2007**, *129*, 3472.
- (21) Kline, R. J.; McGehee, M. D.; Kadnikova, E. N.; Liu, J. S.; Fréchet, J. M. J. *Adv. Mater.* **2003**, *15*, 1519.
- (22) Wang, S. H.; Kappl, M.; Liebewirth, I.; Müller, M.; Kirchhoff, K.; Pisula, W.; Müllen, K. *Adv. Mater.* **2012**, *24*, 417.
- (23) Dallos, T.; Beckmann, D.; Brunklaus, G.; Baumgarten, M. *J. Am. Chem. Soc.* **2011**, *133*, 13898.

- (24) Klauk, H.; Halik, M.; Zschieschang, U.; Schmid, G.; Radlik, W.; Weber, W. *J. Appl. Phys.* **2002**, *92*, 5259.
- (25) Kelley, T. W.; Boardman, L. D.; Dunbar, T. D.; Muyres, D. V.; Pellerite, M. J.; Smith, T. Y. P. *J. Phys. Chem. B* **2003**, *107*, 5877.
- (26) Herwig, P. T.; Müllen, K. *Adv. Mater.* **1999**, *11*, 480.
- (27) Okamoto, T.; Bao, Z. *J. Am. Chem. Soc.* **2007**, *129*, 10308.
- (28) Okamoto, T.; Jiang, Y.; Becerril, H. A.; Hong, S.; Signore, M. L.; Tang, M. L.; Toney, M. F.; Siegrist, T.; Bao, Z. *J. Mater. Chem.* **2011**, *21*, 7078.
- (29) He, M. Q.; Li, J. F.; Sorensen, M. L.; Zhang, F. X.; Hancock, R. R.; Fong, H. H.; Pozdin, V. A.; Smilgies, D. M.; Malliaras, G. G. *J. Am. Chem. Soc.* **2009**, *131*, 11930.
- (30) Li, X. C.; Sirringhaus, H.; Garnier, F.; Holmes, A. B.; Moratti, S. C.; Feeder, N.; Clegg, W.; Teat, S. J.; Friend, R. H. *J. Am. Chem. Soc.* **1998**, *120*, 2206.
- (31) Xiao, K.; Liu, Y. Q.; Qi, T.; Zhang, W.; Wang, F.; Gao, J. H.; Qiu, W. F.; Ma, Y. Q.; Cui, G. L.; Chen, S. Y.; Zhan, X. W.; Yu, G.; Qin, J. G.; Hu, W. P.; Zhu, D. B. *J. Am. Chem. Soc.* **2005**, *127*, 13281.
- (32) Takimiya, K.; Shinamura, S.; Osaka, I.; Miyazaki, E. *Adv. Mater.* **2011**, *23*, 4347.
- (33) Balaji, G.; Valiyaveetil, S. *Org. Lett.* **2009**, *11*, 3358.
- (34) He, M. Q.; Zhang, F. X. *J. Org. Chem.* **2007**, *72*, 442.
- (35) Gao, P.; Beckmann, D.; Tsao, H. N.; Feng, X. L.; Enkelmann, V.; Pisula, W.; Müllen, K. *Chem. Commun.* **2008**, *13*, 1548.
- (36) Gao, P.; Feng, X. L.; Yang, X. Y.; Enkelmann, V.; Baumgarten, M.; Müllen, K. *J. Org. Chem.* **2008**, *73*, 9207.
- (37) Gao, P.; Beckmann, D.; Tsao, H. N.; Feng, X. L.; Enkelmann, V.; Baumgarten, M.; Pisula, W.; Müllen, K. *Adv. Mater.* **2009**, *21*, 213.
- (38) Haryono, A.; Miyatake, K.; Natori, J.; Tsuchida, E. *Macromolecules* **1999**, *32*, 3146.
- (39) Osaka, I.; Abe, T.; Shinamura, S.; Takimiya, K. *J. Am. Chem. Soc.* **2011**, *133*, 6852.
- (40) Facchetti, A. *Chem. Mater.* **2010**, *23*, 733.
- (41) Ito, Y.; Virkar, A. A.; Mannsfeld, S.; Oh, J. H.; Toney, M.; Locklin, J.; Bao, Z. *J. Am. Chem. Soc.* **2009**, *131*, 9396.
- (42) Schmidt, R.; Oh, J. H.; Sun, Y. S.; Deppisch, M.; Krause, A. M.; Radacki, K.; Braunschweig, H.; Könnemann, M.; Erk, P.; Bao, Z.; Würthner, F. *J. Am. Chem. Soc.* **2009**, *131*, 6215.